Revision 2

Potassium isotope fractionation during silicate-carbonatite melt immiscibility and phlogopite fractional crystallization

Ben-Xun Su [1, 2*], Qi-Qi Pan [2, 3], Yang Bai [4], Wen-Jun Li [1], Meng-Meng Cui [1, 2], Kwan-Nang Pang [5]

[1] Key Laboratory of Mineral Resources, Institute of Geology and Geophysics, Chinese Academy of Sciences, Beijing 100029, China

[2] University of Chinese Academy of Sciences, Beijing 100049, China

[3] State Key Laboratory of Lithospheric Evolution, Institute of Geology and Geophysics, Chinese Academy of Sciences, Beijing 100029, China

[4] College of Mining Engineering, Taiyuan University of Technology, Taiyuan 030024, China

[5] Institute of Earth Sciences, Academia Sinica, Taipei, Taiwan

Corresponding author: Ben-Xun Su, subenxun@mail.igcas.ac.cn

This is the peer-reviewed, final accepted version for American Mineralogist, published by the Mineralogical Society of America.
The published version is subject to change. Cite as Authors (Year) Title. American Mineralogist, in press.
DOI: https://doi.org/10.2138/am-2022-8898. http://www.minsocam.org/

ABSTRACT

Potassium (K) isotopes have been used as a tracer of K recycling in the Earth, but K isotope fractionation during magma evolution is poorly constrained. Here, we present K isotope data for a magmatic suite of alkaline silicate-carbonatite affinity, which were formed from melt immiscibility and subsequent phlogopite fractionation. The K isotopic ranges of different rock types are in the following order: alkaline silicate lavas ($\delta^{41}K$ = -0.424‰ to 0.090‰) > carbonatitic silicate lavas ($\delta^{41}K$ = -0.640‰ to -0.035‰) > carbonatites ($\delta^{41}K$ = -0.858‰ and -0.258‰). Phlogopite phenocrysts in the silicate lavas are isotopically lighter ($\delta^{41}K$ = -0.628‰ to -0.534‰) than the lavas in which they occur ($\Delta^{41}K_{Phlogopite\text{-}whole\ rock}$ = -0.502‰ to -0.109‰). Correlations between $\delta^{41}K$ values and chemical proxies of melt immiscibility and phlogopite fractionation indicate that K isotopes are significantly fractionated by both processes at a ~0.6‰ magnitude. Such K isotope variation overlaps the range of $\delta^{41}K$ in arc lavas. Compilations of literature data further confirm the critical roles of melt immiscibility and phlogopite fractionation in K isotope variations of high-K lavas (K_2O > 1 wt.%) from post-collision orogenic and intra-continental settings. In comparison, arc lavas are depleted in K_2O (mostly < 1 wt.%) and lack evidence of significant phlogopite fractionation. The K isotope variations of arc lavas are mainly controlled by their mantle sources, which were metasomatized by melt or fluid released from the subduction slab. Therefore, K recycling and K isotope variation are controlled by distinct mechanisms in various tectonic settings.

Keywords: K isotopes; Silicate rock; Carbonatite; Melt immiscibility; Phlogopite; Fractional crystallization

INTRODUCTION

Potassium (K) displays a large contrast between Earth's crust and mantle in concentration due to its high incompatibility during crust-mantle differentiation (Mittlefehldt, 1998; Lyubetskaya and Korenaga, 2007; Palme and O'Neill, 2007) and is thus a powerful tool to trace crustal recycling and crust-mantle interaction. It is also a fluid-mobile element and its heavy isotopes are in most cases preferentially partitioned into fluids (Mittlefehldt, 1998; Li et al., 2017; Tuller-Ross et al., 2019; Hu et al., 2020; Wang et al., 2021a). Dehydration of the subducting slab releases isotopically heavy melts/fluids to elevate $\delta^{41}K$ shown by arc lavas (Liu et al., 2020; Hu et al., 2021a; Parendo et al., 2022). It has been proposed that further melting of dehydrated slabs is taken to generate magmas showing light K isotopic compositions in tectonic settings far away from subduction trench and arc (Parendo et al., 2022). However, recent studies have revealed that mantle-derived potassic-ultrapotassic rocks in post-collisional and intra-continental environments mostly do not show light K isotope composition compared with arc lavas (Sun et al., 2020; Wang et al., 2021b; Hu et al., 2021a; Liu et al., 2021; Parendo et al., 2022). While heavy K isotopic compositions are generally ascribed to hydrous fluids from subducted slabs, the probable isotope fractionation during magma upward ascent is widely assumed to be negligible

(e.g., Tuller-Ross et al., 2019; Parendo et al., 2022). However, mantle-derived potassic-ultrapotassic rocks commonly undergo fractional crystallization of K-rich minerals such as phlogopite and leucite, which could result in compositionally different isotopic trends compared to other systems dominated by K-poor minerals. Thus, clarifying K isotope fractionation during magma differentiation is essential in using K and its isotopes as a robust geochemical tracer.

Primary carbonatite melts are thought to be alkaline in composition (Chen et al., 2013), but the partitioning and evolution of alkali elements in those melts might be complex due to combined effects of melt immiscibility and fractional crystallization. Mantle-derived alkaline silicate lavas are also commonly rich in K and in some cases associated with carbonatites (Stoppa and Schiazza, 2013). Although many alkaline silicate rock and carbonatite occurrences on the Earth formed from melt immiscibility, some localities lack both rock types at the current level of exposure. In addition, phlogopite, in which K is an important major element, is a common mineral phase in both alkaline silicate rocks and carbonatites. The potential effects of melt immiscibility and phlogopite fractionation on K isotope fractionation have not been widely addressed in earlier studies. The focus of this study is to explore such effects using K isotope compositions of a suite of Cenozoic alkaline silicate rocks and carbonatites in Western Qinling, China.

GEOLOGY BACKGROUND AND SAMPLES

This is the peer-reviewed, final accepted version for American Mineralogist, published by the Mineralogical Society of America.
The published version is subject to change. Cite as Authors (Year) Title. American Mineralogist, in press.
DOI: https://doi.org/10.2138/am-2022-8898. http://www.minsocam.org/

77 Cenozoic potassic-ultrapotassic volcanism is a widespread phenomenon in the Tibetan
78 Plateau and its surroundings (Ding et al., 2003). Western Qinling, located in northeastern Tibetan
79 Plateau, is a unique location where tens of potassic volcanic cones are distributed (Fig. 1; Yu et
80 al., 2005). These volcanic cones are composed of alkaline silicate lavas (also named kamafugite
81 in some literature) and associated coeval carbonatites. This silicate lava-carbonatite association is
82 one of the best-known melt immiscibility examples in the world (Stoppa and Schiazza, 2013).
83 They are believed as melting products of metasomatized mantle sources as evidenced by enriched
84 radiogenic isotopic features (Yu et al., 2004). The well-exposed, accessible outcrops in Western
85 Qinling are mainly distributed in Fenshuiling, Baiguan and Haoti villages (Fig. 1). The
86 carbonatite flow deposits alternate with silicate lavas (Fig. 2a) and mixed silicate lava lapilli and
87 bombs (Fig. 1b, c). The carbonatites have a fine-grained calcite matrix that contains
88 clinopyroxene, phlogopite, and apatite (Stoppa and Schiazza, 2013). The surface-exposed
89 carbonatites are mostly weathered and altered. Some outcrops are dominated by massive silicate
90 lavas. The silicate lavas contain carbonatite nodules in variable sizes (Fig. 1d), and calcite and
91 apatite are the most common Ca-rich phases (Fig. 1e), confirming that the samples are essentially
92 carbonatitic silicate lavas. Some outcrops are relatively pure silicate lavas with mantle peridotite
93 xenoliths (Su et al., 2010). According to field occurrences and mineral assemblages, samples
94 were classified into three groups, namely, pure silicate lava, carbonatite, and carbonatitic silicate
95 lava. All groups show seriate phenocrysts/microcrystals of olivine, phlogopite and clinopyroxene

setting in a matrix of melilite and clinopyroxene laths with intergranular calcite, nepheline/kaliophilite, leucite, phlogopite, perovskite, apatite and titanomagnetite (Yu et al., 2004). The main phenocryst host of K is phlogopite in different types of rocks (Fig. 1f) with decreasing modal abundance from pure silicate lava through carbonatitic silicate lava to carbonatite, while nepheline and leucite microcrystals likely host most K in matrix of the rocks.

In this study, 23 samples were investigated for whole-rock major element analysis, and 19 of them were selected for K isotope analysis using Nu Sapphire collision-cell multi-collector inductively coupled plasma mass spectrometry. Since the carbonatites have been subject to weathering and erosion, only two pristine samples studied here were dug from depth. In addition, phlogopite phenocrysts from three samples were separated for major element and K isotope analyses.

ANALYTICAL METHODS

Whole rock and phlogopite major element analyses

Whole-rock major elements were determined using a Shimadzu X-ray fluorescence spectrometer (XRF-1500) on fused glass beads at the Institute of Geology and Geophysics, Chinese Academy of Sciences (IGGCAS), Beijing, China. Analytical uncertainties were 1-3 % for elements present in concentrations >1 wt.% and about 10 wt.% for elements present in concentrations <1.0 wt.%. Measurement procedures are described in detail by Chu et al. (2009).

This is the peer-reviewed, final accepted version for American Mineralogist, published by the Mineralogical Society of America.
The published version is subject to change. Cite as Authors (Year) Title. American Mineralogist, in press.
DOI: https://doi.org/10.2138/am-2022-8898. http://www.minsocam.org/

115 Major element compositions of phlogopite were measured using JEOL JXA8100 electron
116 probe microanalyzer at IGGCAS. The analytical conditions were accelerating voltage of 15 kV,
117 10 nA beam current, 5 μm beam spot and 10-30 s counting time on peak. The precisions of all
118 analyzed elements were better than 1.5% (1 sigma). Natural jadeite [$NaAlSi_2O_6$] for Na, Al and
119 Si, rhodonite [$MnSiO_3$] for Mn, sanidine [$KAlSi_3O_8$] for K, almandine garnet [$Fe_3Al_2Si_3O_{12}$] for
120 Fe, Cr-diopside [(Mg, Cr) $CaSi_2O_6$] for Ca, olivine [$(Mg, Fe)_2SiO_4$] for Mg, synthetic rutile for
121 Ti, Cr_2O_3 for Cr, and Ni_2Si for Ni were used for standard calibration. A program based on the
122 ZAF procedure was used for matrix corrections. The whole-rock and phlogopite elemental
123 compositions are shown in Tables 1 and 2, respectively.

124 **K isotope analysis**

125 Potassium isotopic analyses were conducted at Metallogenic Elements and Isotopes Lab at
126 IGGCAS, following the protocol described in Li et al. (2022, 2023). Approximately 5-20 mg of
127 sample powders were weighed and digested using mixture of concentrated HNO_3 and HF. The
128 digested sample solutions were evaporated to dryness and then treated sequentially with aqua
129 regia and 6 mol L^{-1} HNO_3. After evaporating the solutions, the final residues were fully
130 dissolved in 0.5 mol L^{-1} HNO_3 twice prior to column separation. The sample solution was loaded
131 onto pre-conditioned 2 mL Bio-Rad AG50W-X8 (200-400 mesh) resin and then eluted with a 15
132 mL of 0.5 mol L^{-1} HNO_3 to remove the matrix elements. The same purification process was
133 repeated twice for silicate lavas and four times for carbonatites to ensure complete matrix

This is the peer-reviewed, final accepted version for American Mineralogist, published by the Mineralogical Society of America.
The published version is subject to change. Cite as Authors (Year) Title. American Mineralogist, in press.
DOI: https://doi.org/10.2138/am-2022-8898. http://www.minsocam.org/

134 removal. The final K solution was redissolved with 2 % HNO_3 ready for measurement. The total
135 procedure blank for K isotope analyses is < 30 ng K, which is negligible compared with tens of
136 μg of K in the solution from sample chemical purification.

137 Potassium isotopic measurements were performed on the Nu Sapphire CC-MC-ICP-MS
138 (Nu Instruments, Wrexham, UK) using the low-energy path. The hexapole collision cell utilizes
139 He and H_2 gas to greatly reduce various Ar-based polyatomic species to very low levels, hence K
140 isotopic ratios can be measured in the low-resolution mode. An auto-sampler SC-2DX
141 (Elemental Scientific, USA) was connected to an Apex Omega desolvation nebulizer (Elemental
142 Scientific, U.S.A.) system for sample introduction. One Faraday cup is connected to a pre-
143 amplifier fitted with a 10^{10} Ω resistor for collection of $^{39}K^+$ ion beam, while the other two
144 Faraday cups using 10^{11} Ω resistors collect $^{41}K^+$ and mass 40 beams, respectively. Potassium
145 isotopic data are reported in δ notation relative to SRM 3141a, using the sample-standard
146 bracketing technique for instrumental mass fractionation correction (Hu et al., 2018):

$$\delta^{41}\mathrm{K}\,(‰) = \left[\frac{\left(^{41}\mathrm{K}/^{39}\mathrm{K}\right)_{\mathrm{sample}}}{\left(^{41}\mathrm{K}/^{39}\mathrm{K}\right)_{\mathrm{standard}}} - 1\right] \times 1000$$

147 The K concentration of each sample and standard was matched to within 5%. Each analysis
148 consisted of 1 block of 50 cycles with 4 s integrations. Five to seven repeated analyses were
149 conducted on each sample solution. The K isotope results of whole rocks and phlogopite are
150 shown in Table 3. Four geostandards analyzed during the course of this study yield values in

This is the peer-reviewed, final accepted version for American Mineralogist, published by the Mineralogical Society of America.
The published version is subject to change. Cite as Authors (Year) Title. American Mineralogist, in press.
DOI: https://doi.org/10.2138/am-2022-8898. http://www.minsocam.org/

151 good agreement with literature (Xu et al., 2019; Li et al., 2020, 2022; Chen et al., 2022, Moynier
152 et al., 2022). Replicated analyses of nine samples are consistent within analytical uncertainty.
153 The long-term (six months) precision, based on multiple measurements of BCR-2 geostandard, is
154 ~0.04‰ (2SD; Li et al., 2022).
155
156 **RESULTS**
157 The pure silicate lava samples have SiO_2 contents of 39.9-42.1 wt.%, CaO of 12.1-12.8
158 wt.%, TiO_2 of 2.93-3.76 wt.%, Na_2O+K_2O of 5.15-6.70 wt.%, and K_2O of 1.35-3.14 wt.% with
159 K_2O/Na_2O ratios of 0.36-0.88 (Table 1). The low LOI values (loss of ignition, 0.42-1.74 wt.%),
160 together with pristine mineral assemblages, indicate that these samples are free of alteration.
161 Their $\delta^{41}K$ values range from -0.424‰ to 0.090‰ (Table 3). The two carbonatite samples are
162 significantly rich in CaO and depleted in SiO_2, TiO_2 and alkali components in contrast to silicate
163 lavas (Fig. 3a-c). They have $\delta^{41}K$ values of -0.858‰ and -0.258‰, respectively. The carbonatitic
164 silicate lavas have intermediate elemental compositions between the silicate lavas and the
165 carbonatites (Fig. 3a-c) and have $\delta^{41}K$ values ranging from -0.640‰ to -0.035‰ (Table 3). Their
166 relatively higher LOI (1.10-5.41 wt.%; Table 1) are related to carbonatitic components and
167 phlogopite contents. Phlogopite phenocrysts in the silicate lavas and carbonatitic silicate lavas are
168 rich in TiO_2 (3.60-12.0 wt.%) and variable in K_2O contents of 7.68-10.2 wt.% (Table 2; Yu,
169 1994). They have low K isotope ratios ($\delta^{41}K$ = -0.628‰ to -0.534‰) relative to the whole rocks.

This is the peer-reviewed, final accepted version for American Mineralogist, published by the Mineralogical Society of America.
The published version is subject to change. Cite as Authors (Year) Title. American Mineralogist, in press.
DOI: https://doi.org/10.2138/am-2022-8898. http://www.minsocam.org/

170

171 # DISCUSSION

172 ## Melt immiscibility and phlogopite fractionation in genesis of the Western Qinling lavas

173 Coeval silicate and carbonatite lavas in Western Qinling show close spatial affinity because
174 they are interlayered (Fig. 2a), and contain relics of their counterparts at various scales of field
175 outcrop, hand specimen, and micro-texture (Fig. 2b-e). The petrological characteristics of both
176 are compatible with geochemical compositions. The silicate lavas free of carbonatitic
177 components have notably higher SiO_2 contents and lower CaO than the carbonatites, while the
178 carbonatitic silicate lavas with observed carbonatitic components have intermediate oxide
179 contents between the silicate lavas and the carbonatites (Fig. 3a). These features are comparable
180 to typical silicate-carbonatite associations worldwide (e.g., Woolley and Kjarsgaard, 2008;
181 Stoppa and Schiazza, 2013), suggesting the studied lava samples here had experienced silicate-
182 carbonatite melt immiscibility but that the two immiscible melts were not completely separated.
183 Compositional differences of major elements such as SiO_2 and CaO between the rocks (Fig. 3a)
184 confirm that the silicate lavas and the two carbonatite samples could represent two immiscible
185 melt end-members, respectively, while the carbonatitic silicate samples are products of
186 incompletely-separated melts. Lower K_2O and Na_2O+K_2O contents and higher K_2O/Na_2O ratios
187 in the carbonatites than those in the silicate lavas (Fig. 3b, c) together with good correlation
188 between TiO_2 and K_2O (Fig. 3d) demonstrate that Ti and alkali components with relatively less K

This is the peer-reviewed, final accepted version for American Mineralogist, published by the Mineralogical Society of America.
The published version is subject to change. Cite as Authors (Year) Title. American Mineralogist, in press.
DOI: https://doi.org/10.2138/am-2022-8898. http://www.minsocam.org/

than Na were preferentially partitioned into silicate melts. This is consistent with some experimental observations (Martin et al., 2013).

Potassium behaves incompatible during mafic magma differentiation. Its contents in evolved magmas are generally elevated by fractional crystallization of K-free or -poor phases (e.g., olivine, clinopyroxene and spinel), generating positive correlations with SiO_2 content. However, fractional crystallization of K-rich phases (e.g., phlogopite) could deplete the residual liquid in K_2O, creating a negative correlation with SiO_2 as observed in Fig. 3c. The presence of phlogopite phenocrysts (Fig. 1f) and in places megacrysts (Yu et al., 2004) in all the studied rocks, together with their chemical variations (Fig. 3b, c), reveal that the investigated rocks underwent fractional crystallization of Ti-rich phlogopite. The composition of phlogopite resulted in significant decrease of K_2O and TiO_2 contents and K_2O/Na_2O ratios, which are distinctive from the compositional changes resulted from melt immiscibility (Fig. 3). Hence, the different evolutionary trends among the three melt types outlined in Fig. 3 are not only dependent on the degree of phlogopite fractionation but also their K_2O contents after melt immiscibility.

K isotope fractionation during melt immiscibility and phlogopite fractionation

Previous petrological and geochemical studies, including Sr-Nd-Pb-Hf isotopes, have suggested that the parental mamgas of the lavas were derived from a common mantle source via low degree partial melting (Yu et al., 2004; Dai et al., 2017) and experienced crustal-level melt immiscibility (Stoppa and Schiazza, 2013). The silicate lavas in this study are suitable to evaluate

K isotope fractionation during magma evolution because they contain significant phlogopite and have the highest contents and largest variations of K_2O (Figs. 2f, 3c). The phlogopite phenocrysts have lighter K isotopic compositions than the silicate host rocks (Table 3), and their whole-rock $\delta^{41}K$ values are well correlated with chemical indicators (e.g., K_2O/Na_2O, Na_2O+K_2O and TiO_2) of phlogopite fractional crystallization. This suggests that phlogopite prefers to incorporate light K isotopes from melt during crystallization, and thus phlogopite fractional crystallization resulted in heavy K isotope enrichment in evolved melts with 0.6‰ magnitude fractionation in $\delta^{41}K$. Similar variation trends of $\delta^{41}K$ values are also observed in individual carbonatites and crabonatitic silicate lavas (Fig. 4).

To further verify this inference, we conducted quantitative modeling based on the Rayleigh fractionation and mixing modeling for the silicate lavas (Fig. 5a). The equation that governs isotopic fractionation in a Rayleigh distillation process is:

$$\delta^{41}K_{melt} = \left(\delta^{41}K_0 + 1000\right) f^{(\alpha-1)} - 1000$$

where the $\delta^{41}K_0$ is the initial K isotope of melts, and is set as -0.43‰, which is the mean $\delta^{41}K$ value of the bulk silicate earth (Tuller-Ross et al., 2019). The initial K_2O contents of melts is set as 2.0 wt.%. The fraction of K_2O remaining in the melt and other phases is $f = (F \times C_{melt}) / C_0$, where C_{melt} and C_0 represent the K_2O concentration in the remaining melts with other phases and the initial melts, and the F is the fraction of melts remaining. The fractionation factor α is calculated by:

This is the peer-reviewed, final accepted version for American Mineralogist, published by the Mineralogical Society of America.
The published version is subject to change. Cite as Authors (Year) Title. American Mineralogist, in press.
DOI: https://doi.org/10.2138/am-2022-8898. http://www.minsocam.org/

$$\Delta^{41}\mathrm{K}_{phl-melt} = \delta^{41}\mathrm{K}_{phl} - \delta^{41}\mathrm{K}_{melt} \approx 10^3 \ln \alpha_{phl-melt}$$

Where the average phl-melt fractionation factors ($\Delta^{41}K_{phl\text{-}melt} = \delta^{41}K_{phl}\text{-}\delta^{41}K_{melt}$) is -0.146‰ in our model, and is calculated by average δ^{41}K values of phlogopite (-0.576‰) and basalts (-0.430‰).

In mixing model, the equation that governs mixing of 2 end-members is:

$$C_A = (C_A)_{melt,0} \times F_{melt,0} + (C_A)_{phl} \times F_{phl}$$

Where C_A is the fraction of K_2O from the end member 1, end member 2, and the mixing phase, and the F is the fraction in each member. The lines in Fig. 5a represent calculated mixing lines between the residual melt and phlogopite. Phlogopite from the eruption samples have the K_2O contents from 7.79 to 9.35 wt.%, and the average composition of K_2O = 8.72 wt.% has been used as an end-member in the mixing calculation. The K isotope composition of unmodified lava can be calculated by:

$$\delta^{41}\mathrm{K}_{lava} = \delta^{41}\mathrm{K}_{residual\ melts,0} \times (C)_{residual\ melts,0} \times F_{residual\ melts,0} + \delta^{41}\mathrm{K}_{Phl,0} \times (C)_{Phl,0} \times F_{Phl,0}$$

where the $\delta^{41}K_{residual\ melt,\ 0}$ and $\delta^{41}K_{Phl}$ could identify with the $\delta^{41}K_0$ and $\delta^{41}K_{lava}$ in the model for Rayleigh distillation.

The modelling results demonstrate that the obtained K isotopic compositions of the silicate lavas are not a mixture between phlogopite and evolved melts but resulted from phlogopite fractionation. The slightly high K_2O contents of the samples than the modeling results (Fig. 5a) are likely due to K elevation by crystallization of K-free mineral (such as olivine and

246 clinopyroxene).

247 Assuming that the silicate lava and the carbonatite samples with the lowest $\delta^{41}K$ values (-
248 0.424‰ and -0.858‰, respectively) represent melts with the least degree of phlogopite fractional
249 crystallization, K isotopes could be fractionated at a magnitude of 0.43‰ during melt
250 immiscibility. Particularly for silicate melts, both melt immiscibility and phlogopite fractional
251 crystallization significantly increase their $\delta^{41}K$ values up to 1‰. Since the carbonatites are
252 depleted in K relative to the silicate lavas, crystallization of minor phlogopite would produce
253 larger fractionations as indicated by the K isotope compositions of the two samples (Fig. 4). The
254 differences in K_2O and TiO_2 contents between the two carbonatite samples may indicate variable
255 degrees of phlogopite fractional crystallization, thus resulting in a large range in K isotopic
256 composition. The isotopic differences between phlogopite and host rocks imply that heavy K
257 isotopes for K mass balance are probably hosted in matrix nepheline because nepheline is
258 predicted to have higher $10^3 ln\beta$ than phlogopite (Li et al., 2019). This significant K isotope
259 variation during magma differentiation overlaps the K isotope ranges of mantle-derived magmas
260 reported so far (Tuller-Ross et al., 2019; Sun et al., 2020; Hu et al., 2021b; Ionov and Wang,
261 2021; Wang et al., 2021b; Parendo et al., 2022) (Fig. 5b, c). Therefore, the possible effects of
262 melt immiscibility and phlogopite fractional crystallization should be considered prior to using K
263 isotopes to trace magma sources.

264 In addition to phlogopite, leucite is also a common K-rich phase in mantle-derived potassic

265 volcanic rocks (Bergman, 1987). and leucite + phlogopite may coexist in lamproites such as those
266 from the Alpine-Himalayan orogenic belt (Wang et al., 2021b). These lamproite samples fall
267 along the trend line of phlogopite fractional crystallization (Wang et al., 2021b; Fig. 5b, c),
268 implying that their K isotope variations are probably partially addressed by phlogopite
269 crystallization in addition to source control as discussed by Wang et al. (2021b). The data
270 presented in this study show mixed features of both processes. Moreover, alkali lavas elsewhere
271 containing leucite with rare phlogopite are also generally following the trend of phlogopite
272 fractional crystallization (Sun et al., 2020; Wang et al., 2021b; Fig. 5b, c). Although it has not yet
273 (to our knowledge) been measured for K isotopes, leucite is predicted to have an even stronger
274 preference for isotopically light K than phologipite (Li et al., 2019). This may indicate that
275 leucite plays a similar role to phlogopite in K isotope fractionation in alkali igneous systems.
276

277 **IMPLICATIONS**

278 Unlike the alkali volcanic rocks in orogenic or intra-continental settings, typical arc lavas,
279 mostly sub-alkaline in nature, are relatively poor in K (mostly K_2O < 1.5 wt.%) and rich in Na
280 with low K_2O/Na_2O ratio (< 1) (Fig. 5b, c). Arc lavas tend to crystallize hornblende and/or
281 clinopyroxene, rather than phlogopite, to form hornblendite and/or clinopyroxenite cumulates in
282 arc crust (DeBari and Coleman, 1989; Cui et al., 2020). Crystallization of these K-poor minerals,
283 instead of K-rich phases, increases K_2O contents and thus K_2O/Na_2O ratios in the evolved melts

and would not cause significant effect on K isotope ratios. Therefore, K isotope compositions of arc lavas should reflect those of the mantle sources from which the lavas derived (Hu et al., 2021b; Ionov and Wang, 2021; Parendo et al., 2022). Hydrous fluids released from subducting slabs incorporate more heavy K isotopes into metasomatized mantle wedge (Liu et al., 2020, 2021; Sun et al., 2020; Ionov and Wang, 2021; Wang et al., 2021b), but at initial stages only minor amount of K is released because of the low K content in most arc lavas. The subducting slab and thus slab melt would become relatively K-rich and isotopically light, resulting in progressively more K-rich and isotopically light metasomatized mantle with distance away from the subduction trench (Fig. 6). This mechanism is consistent with K isotope variations in typical arc lavas with higher δ^{41}K values in frontal arc than that in rear arc (Parendo et al., 2022). Intra-continental alkaline to sub-alkaline silicate lavas, if derived from stagnated slab melt-metasomatized mantle via low-degree partial melting, should be rich in K and have very light K isotopic composition (Wang et al., 2021b; Sun et al., 2020). This contrasts with the low K content and generally heavier K isotope composition of ocean island basalts (Tuller-Ross et al., 2019) and arc lavas (Hu et al., 2021; Parendo et al., 2022), which are primarily controlled by source compositions. As a consequence, K recycling and its isotopic variation are controlled by distinct mechanisms in various tectonic settings.

Acknowledgements We appreciate constructive reviews from editor William Peck and two anonymous reviewers, which significantly improved the quality of the paper. This work was financially supported by the Experimental Technology Innovation Fund of the Institute of Geology and Geophysics, Chinese Academy of Sciences (TEC 202103), and the Youth Innovation Promotion Association, Chinese Academy of Sciences.

References

Bergman, S.C., 1987. Lamproites and other potassium-rich igneous rocks: a review of their occurrence, mineralogy and geochemistry. Geological Society, London, Special Publications 30, 103-190.

Chen H., Saunders N.J., Jerram M., Halliday A.N., 2021. High-precision potassium isotopic measurements by collision cell equipped MCICPMS. Chemical Geology 578, 120281.

Chen, H., Tian, Z., Tuller-Ross, B., Korotev-Randy, L., Wang, K., 2019. High-precision potassium isotopic analysis by MC-ICP-MS: An inter-laboratory comparison and refined K atomic weight. Journal of Analytical Atomic Spectrometry 34, 160-171.

Chen, W., Kamenetsky, V.S., Simonetti, A., 2013. Evidence for the alkaline nature of parental carbonatite melts at Oka complex in Canada. Nature Communications 4, 1-6.

Chu Z.Y., Wu F.Y., Walker R.J., Rudnick R.L., Pitcher L., Puchtel I.S., Yang Y.H., Wilde S.A., 2009. Temporal evolution of the lithospheric mantle beneath the eastern North China Craton. Journal of Petrology 50, 1857-1898.

322 Cui, M.M., Bai, Y., Su, B.X., Xiao, Y., Wang, J., Pan, Q.Q., Gao, D.L., 2020. Characteristics,
323 petrogenesis and metallogenesis of Alaskan-type complexes. Mineral Deposits 39, 397-418.
324 Dai, L.Q., Zhao, Z.F., Zheng, Y.F., An, Y.J., Zheng, F., 2017. Geochemical distinction between
325 carbonate and silicate metasomatism in generating the mantle sources of alkali basalts.
326 Journal of Petrology 58, 863-84.
327 DeBari, S.M., Coleman, R.G., 1989. Examination of the deep levels of an island arc: Evidence
328 from the Tonsina ultramafic-mafic assemblage, Tonsina, Alaska. Journal of Geophysical
329 Research: Solid Earth 94, 4373-4391.
330 Ding, L., Kapp, P., Zhong, D., Deng, W., 2003. Cenozoic volcanism in Tibet: Evidence for a
331 transition from oceanic to continental subduction. Journal of Petrology 44, 1833-1865.
332 Hu, Y., Chen, X.Y., Xu, Y.K., Teng, F.Z., 2018. High precision analysis of potassium isotopes
333 by HR-MC-ICPMS. Chemical Geology 493, 100-108.
334 Hu, Y., Teng, F.Z., Chauvel, C., 2021a. Potassium isotopic evidence for sedimentary input to the
335 mantle source of Lesser Antilles lavas. Geochimica et Cosmochimica Acta 295, 98-111.
336 Hu, Y., Teng, F.Z., Helz, R.T., Chauvel, C., 2021b. Potassium isotope fractionation during
337 magmatic differentiation and the composition of the mantle. Journal of Geophysical Research-
338 Solid Earth 126, e2020JB021543.
339 Hu, Y., Teng, F.Z., Plank, T., Chauvel, C., 2020. Potassium isotopic heterogeneity in subducting
340 oceanic plates. Science Advance 6, eabb2472.
341 Ionov, D.A., Wang, K., 2021. Potassium distribution and isotope composition in the lithospheric
342 mantle in relation to global Earth's reservoirs. Geochimica et Cosmochimica Acta 309, 151-
343 170.
344 Li X., Han G., Zhang Q., Miao Z., 2020. An optimal separation method for high-precision K
345 isotope analysis by using MC-ICP-MS with a dummy bucket. Journal of Analytical Atomic
346 Spectrometry 35, 1330-1339.

Li, W., Cui, M., Pan, Q., Wang, J., Gao, B., Liu, S., Yuan, M., Su, B., Zhao, Y., Teng, F.Z., Han, G., 2022. High-precision potassium isotope analysis using the Nu Sapphire collision cell (CC)-MC-ICP-MS. Science China Earth Sciences 65, 1510-1521.

Li, W.J., Zhao, Y., Su, B.X., Gao, B.Y., Wang, J., Liu, S.K., 2023. Experimental investigation of improved tolerance for concentration mismatch in potassium isotope analysis on a hexapole collision cell MC-ICP-MS (Nu Sapphire). Journal of Analytical Atomic Spectrometry 38, 603-608.

Li, W., Kwon, K.D., Li, S., Beard, B.L., 2017. Potassium isotope fractionation between K-salts and saturated aqueous solutions at room temperature: Laboratory experiments and theoretical calculations. Geochimica et Cosmochimica Acta 214, 1-13.

Li, Y., Wang, W., Wu, Z., Huang, S., 2019. First-principles investigation of equilibrium K isotope fractionation among K-bearing minerals. Geochimica et Cosmochimica Acta 264, 30-42.

Liu, H., Xue, Y.Y., Wang, K., Sun, W.D., Wang, K., 2021., Contributions of slab-derived fluid to ultrapotassic rocks indicated by K isotopes. Lithos 396-397, 106202.

Liu, H.Y., Wang, K., Sun, W.D., Xiao, Y.L., Xue, Y.Y., Tuller-Ross, B., 2020. Extremely light K in subducted low-T altered oceanic crust: Implications for K recycling in subduction zone. Geochimica et Cosmochimica Acta 277, 206-223.

Lyubetskaya, T., Korenaga, J., 2007. Chemical composition of Earth's primitive mantle and its variance: 1. Method and results. Journal of Geophysical Research: Solid Earth 112, B03211.

Martin, L.H., Schmidt, M.W., Mattsson, H.B., Guenther, D., 2013. Element partitioning between immiscible carbonatite and silicate melts for dry and H_2O-bearing systems at 1-3 GPa. Journal of Petrology 54, 2301-2338.

Mittlefehldt, D.W., 1998. Potassium. In: Geochemistry. Encyclopedia of Earth Science. Springer Netherlands, Dordrecht, pp. 522.

372 Morgan, L.E., Santiago-Ramos, D.P., Davidheiser-Kroll, B., Faithfull, J., Lloyd, N.S., Ellam,
373 R.M., Higgins, J.A., 2018. High-precision $^{41}K/^{39}K$ measurements by MC-ICP-MS indicate
374 terrestrial variability of $\delta^{41}K$. Journal of Analytical Atomic Spectrometry 33, 175-186.

375 Moynier F., Hu Y., Wang K., Zhao Y., Gérard Y., Deng Z., Moureau J., Li W., Simon J.I., Teng
376 F.Z., 2021. Potassium isotopic composition of various samples using a dual-path collision
377 cell-capable multiple-collector inductively coupled plasma mass spectrometer, Nu instruments
378 Sapphire. Chemical Geology 571, 120144.

379 Palme, H., O'Neill, H.S.C., 2007. Cosmochemical Estimates of Mantle Composition, in: Holland,
380 H.D., Turekian, K.K. (Eds.), Treatise on Geochemistry. Pergamon, Oxford, 1-38.

381 Parendo, C.A., Jacobsen, S.B., Kimura, J.I. and Taylor, R.N., 2022. Across-arc variations in K-
382 isotope ratios in lavas of the Izu arc: Evidence for progressive depletion of the slab in K and
383 similarly mobile elements. Earth and Planetary Science Letters 578, 117291.

384 Stoppa, F., Schiazza, M., 2013. An overview of monogenetic carbonatitic magmatism from
385 Uganda, Italy, China and Spain: volcanologic and geochemical features. Journal of South
386 American Earth Sciences 41, 140-159.

387 Su, B.X., Zhang, H.F., Sakyi, P.A., Ying, J.F., Tang, Y.J., Yang, Y.H., Qin, K.Z., Xiao, Y., Zhao,
388 X.M., 2010. Compositionally stratified lithosphere and carbonatite metasomatism recorded in
389 mantle xenoliths from the Western Qinling (Central China). Lithos 116, 111-128.

390 Sun, Y., Teng, F.Z., Hu, Y., Chen, X.Y., Pang, K.N., 2020. Tracing subducted oceanic slabs in
391 the mantle by using potassium isotopes. Geochimica et Cosmochimica Acta 278, 353-360.

392 Tuller-Ross, B., Marty, B., Chen, H., Kelley, K.A., Lee, H., Wang, K., 2019. Potassium isotope
393 systematics of oceanic basalts. Geochimica et Cosmochimica Acta 259, 144-154.

394 Wang, K., Jacobsen, S.B., 2016. An estimate of the Bulk Silicate Earth potassium isotopic
395 composition based on MC-ICP-MS measurements of basalts. Geochimica et Cosmochimica
396 Acta 178, 223-232.
397 Wang, K., Li, W., Li, S., Tian, Z., Koefoed, P., Zheng, X.Y., 2021a. Geochemistry and
398 cosmochemistry of potassium stable isotopes. Geochemistry 81, 125786.
399 Wang, Z.Z., Teng, F.Z., Prelevi´c, D., Liu, S.A., Zhao, Z., 2021b. Potassium isotope evidence for
400 sediment recycling into the orogenic lithospheric mantle. Geochemical Perspective Letters 18,
401 43-47.
402 Woolley, A.R., Kjarsgaard, B.A., 2008. Paragenetic types of carbonatite as indicated by the
403 diversity and relative abundances of associated silicate rocks: evidence from a global database.
404 The Canadian Mineralogist 46, 741-752.
405 Xu, Y.K., Hu, Y., Chen, X.Y., Huang, T.Y., Sletten, R.S., Zhu, D., Teng, F.Z., 2019. Potassium
406 isotopic compositions of international geological reference materials. Chemical Geology 513,
407 101-107.
408 Yu, X.H., 1994. Titanphlogopite from the Cenozoic Alkaline volcanic rock in western Qinling,
409 Gansu province. Acta Petrologica et Mineralogica 13, 319-327.
410 Yu, X.H., Zhao, Z.D., Mo, X.X., Wang, Y.L., Xiao, Z., Zhu, D.Q., 2004. Trace element, REE
411 and Sr, Nd, Pb isotopic geochemistry of Cenozoic kamafugites and carbonatite from west
412 Qinling, Gansu Province: Implication of plume-lithosphere interaction. Acta Petrologica
413 Sinica 20, 483-494 (in Chinese with English abstract).
414 Yu, X.H., Zhao, Z.D., Mo, X.X., Zhou, S., Zhu, D.Q., Wang, Y.L., 2005. $^{40}Ar/^{39}Ar$ dating for
415 Cenozoic kamafugites from western Qinling in Gansu Province. Chinese Science Bulletin 50,
416 2638-2643.

417

418 **Figures**

419 Fig. 1 (a) Distribution of silicate lavas and carbonatites in Western Qinling, China.

420

421 Fig. 2 (a-c) Slices of silicate lavas occurring as interlayer, nodule and block in carbonatite bodies.
422 (d) Carbonatite components occurring as nodules of variable sizes in carbonatitic silicate lavas. (f)
423 Back-scattered electron image showing carbonatite components occurring as calcite (Cal) and
424 apatite (Apat) together with olivine (Ol) and clinopyroxene (Cpx) phenocrysts in silicate lavas.
425 (g) Occurrence of phlogopite (Phl) phenocryst in silicate lavas.

426

427 Fig. 3 Correlation diagrams of (a) SiO_2 vs. CaO, (b) Na_2O+K_2O vs. K_2O/Na_2O, (c) SiO_2 vs. K_2O
428 and (d) K_2O vs. TiO_2 indicate incomplete separation between silicate and carbonatite melts in
429 carbonatitic silicate lava samples relative to pure silicate and carbonatite samples, and significant
430 phlogopite (Phl) fractionation in the samples. Phlogopite phenocryst data are available in Table 2
431 and Yu (1994).

432

433 Fig. 4 Correlation diagrams of (a) Na_2O+K_2O, (b) K_2O/Na_2O, and (c) TiO_2 vs. $\delta^{41}K$ indicate
434 significant fractionation of K isotopes during melt immiscibility and phlogopite fractionation.
435 Legends same as Fig. 2.

436

Fig. 5 (a) Modeling of K isotopic variations during magmatic differentiation in silicate lavas. Solid lines represent calculated K isotopic compositions of residual melts during phlogopite fractional crystallization by assuming a Rayleigh distillation process. Dashed black lines represent calculated mixing lines between the residual melt and phlogopite phenocrysts. The $\delta^{41}K$ values of primary melt and phlogopite are assumed as -0.430‰ (Wang and Jacobsen, 2016; Hu et al., 2018; Morgan et al., 2018; Chen et al., 2019; Xu et al., 2019; Sun et al., 2020) and -0.576‰ (Table 3; average K isotopic compositions of phlogopite separates), with phlogopite-melt fractionation factors ($\Delta\delta^{41}K_{phlogopite\text{-}melt} = \delta^{41}K_{phlogopite} - \delta^{41}K_{melt}$) of -0.146‰. The K_2O contents of primary melt are assumed as 2 wt.% following the average K_2O contents of Northeast China lavas (Sun et al., 2020), and the colored stars represent the increased 33%, 50% and 60% K_2O contents in melts caused by K-poorly mineral cumulations prior to phlogopite. The phlogopite K_2O contents of 8.72 wt.% are calculated by average K_2O contents. (b, c) Comparisons of K isotopes between mantle-derived rocks from various tectonic settings. Solid line with arrow indicates a trend of phlogopite fractional crystallization, and the dashed line with arrow indicates a trend of mantle source variation with distance to subduction trend.

Fig. 6 Simplified model showing K and its isotope behavior from arc to intra-continent setting. Minor element K with preferential heavy isotopes is released from subducting slab in arc setting, resulting in isotopically light dehydrated slab and decreasing tendency of $\delta^{41}K$ value in

456 metasomatized mantle and thus arc lavas with distance away from trench. Due to K depletion,
457 amphibole rather than phlogopite is the dominant K-host phase crystallized from arc lavas and
458 the fractional crystallization does not induce significant K isotope fractionation. Melting of
459 residual slab in depth generates K-rich and isotopically light melts to account for low-$\delta^{41}K$
460 features of primary intra-continental potassic-ultrapotassic lavas, while melt immiscibility and
461 phlogopite fractional crystallization lead to significant K isotope fractionation and thus relatively
462 large isotopic compositional variations.

Table 1 Major element compositions (wt.%) of carbonatitic silicate lavas, silicate lavas and carbonatites from Western Qinling, China

Sample	SiO_2	TiO_2	Al_2O_3	TFe_2O_3	MnO	MgO	CaO	Na_2O	K_2O	P_2O_5	LOI	Total
Carbonatitic silicate lava												
BG1	39.7	3.77	9.07	12.4	0.17	12.8	12.6	3.15	2.66	1.29	1.10	98.7
BG2	39.1	3.14	7.93	11.1	0.16	16.0	12.9	1.84	1.23	1.21	4.44	99.0
BG3	39.9	3.19	7.94	11.4	0.15	15.5	12.5	2.44	1.43	1.16	3.42	99.0
BG4	38.9	3.21	7.77	11.2	0.16	15.7	12.6	1.47	0.97	1.49	5.41	98.8
BG5	38.4	3.07	7.42	11.2	0.15	18.3	12.2	1.13	0.70	1.40	5.09	99.1
BG6	38.4	3.06	7.47	11.2	0.15	18.3	12.2	1.07	0.68	1.41	4.99	98.9
Silicate lava												
HT1	40.2	3.73	9.49	12.3	0.17	12.4	12.3	3.56	2.99	1.09	0.50	98.7
HT2	40.2	3.64	9.49	12.1	0.16	12.6	12.3	3.48	2.95	1.09	0.60	98.6
HT3	40.1	3.65	9.37	12.2	0.17	12.7	12.3	3.47	2.95	1.12	0.64	98.7
HT3-r	40.0	3.64	9.34	12.2	0.16	12.7	12.4	3.49	2.93	1.12	0.60	98.5
HT4	41.0	3.30	9.34	12.0	0.16	12.7	12.2	3.54	1.99	1.10	1.40	98.7
HT5	39.9	3.66	9.55	12.1	0.16	12.4	12.2	3.56	3.03	1.07	0.42	98.1
HT5-r	40.0	3.68	9.46	12.1	0.17	12.5	12.2	3.58	3.01	1.07	0.42	98.2
HT6	41.3	3.00	9.21	11.4	0.16	12.3	12.4	3.66	1.62	1.15	1.76	97.9
HT7	40.1	3.68	9.44	12.2	0.17	12.2	12.2	3.42	2.89	1.01	0.96	98.2
HT8	42.1	2.93	9.16	11.1	0.16	12.8	12.6	3.80	1.35	1.17	1.74	98.9
HT9	39.9	3.76	9.47	12.3	0.17	12.4	12.3	3.56	2.97	1.08	0.62	98.5
HT10	40.4	3.68	9.50	12.1	0.17	12.3	12.3	3.54	3.05	1.01	0.76	98.8
HT11	41.9	3.08	9.21	11.4	0.16	12.8	12.8	3.74	1.59	1.25	1.58	99.5
HT12	40.6	3.70	9.46	12.2	0.17	12.4	12.4	3.35	2.95	1.05	0.96	99.2
HT13	40.2	3.65	9.66	12.1	0.17	12.1	12.1	3.56	3.14	0.97	0.84	98.4
HT14	40.0	3.68	9.43	12.1	0.17	12.5	12.4	3.50	2.94	1.10	0.60	98.4
HT15	40.3	3.69	9.55	12.2	0.17	12.3	12.2	3.56	3.04	1.00	0.66	98.7
HT15-r	40.3	3.68	9.52	12.2	0.17	12.4	12.2	3.53	3.04	0.99	0.64	98.6
Carbonatite												
FS01	22.4	2.26	5.56	8.00	0.11	5.27	26.3	0.17	1.04	1.31	27.9	100
FS01-r	22.4	2.26	5.56	7.98	0.11	5.28	26.3	0.15	1.04	1.31	27.8	100
FS02	30.8	2.89	6.73	10.5	0.15	3.62	21.5	0.12	0.59	0.96	22.4	100

Note: r, replicated analysis; LOI, loss of ignition.

This is the peer-reviewed, final accepted version for American Mineralogist, published by the Mineralogical Society of America.
The published version is subject to change. Cite as Authors (Year) Title. American Mineralogist, in press.
DOI: https://doi.org/10.2138/am-2022-8898. http://www.minsocam.org/

Table 2 Phlogopite phenocrysts in silicate lavas from Western Qinling, China

SiO_2	39.4	36.1	35.8	36.1	38.1	36.5	37.4	36.7	37.8	37.3	38.1	35.6	41.8	42.4
TiO_2	8.12	9.48	9.29	9.55	8.28	9.27	9.24	9.57	8.78	9.57	8.40	9.69	7.30	7.28
Al_2O_3	9.48	11.3	10.8	11.4	9.88	10.8	10.4	11.0	10.0	10.8	9.50	11.5	7.68	7.36
Cr_2O_3	0.00	0.02	0.03	0.03	0.03	0.00	0.00	0.04	0.05	0.00	0.01	0.03	0.20	0.14
FeO	10.1	9.02	9.13	9.06	9.49	9.59	9.82	9.28	9.61	9.12	10.6	9.45	6.38	6.81
MnO	0.10	0.08	0.08	0.09	0.07	0.05	0.07	0.07	0.06	0.08	0.04	0.07	0.06	0.05
MgO	17.0	15.6	15.6	16.0	16.1	15.3	15.5	15.7	16.0	16.1	17.0	15.7	20.0	19.9
CaO	0.03	0.07	0.01	0.00	0.01	0.00	0.02	0.04	0.05	0.00	0.03	0.01	0.04	0.04
Na_2O	0.39	0.37	0.37	0.34	0.32	0.34	0.39	0.34	0.29	0.36	0.32	0.30	0.62	0.68
K_2O	9.35	7.98	8.02	7.91	8.89	8.12	8.60	8.33	9.02	8.54	9.10	7.79	9.40	9.93
NiO	0.00	0.03	0.03	0.08	0.07	0.08	0.05	0.04	0.03	0.08	0.03	0.02	0.05	0.04
Total	93.9	90.1	89.1	90.5	91.2	90.1	91.4	91.0	91.8	91.9	93.1	90.1	93.5	94.7

This is the peer-reviewed, final accepted version for American Mineralogist, published by the Mineralogical Society of America.
The published version is subject to change. Cite as Authors (Year) Title. American Mineralogist, in press.
DOI: https://doi.org/10.2138/am-2022-8898. http://www.minsocam.org/

Table 3 Potassium isotope ratios (‰) of standards and carbonatitic silicate lavas, silicate lavas and carbonatites, and phlogopite phenocrysts in silicate lavas from Western Qinling, China

Sample	Comment	$\delta^{41}K$	2SD
Standard			
BCR-2		-0.413	0.037
Replicated		-0.441	0.050
BCR-2		-0.447	0.035
GBW07103(GSR1)		-0.511	0.041
Replicated		-0.481	0.027
DNC-2		-0.298	0.032
G2		-0.449	0.014
Carbonatitic silicate lava			
BG1	Whole rock	-0.640	0.019
Duplicated		-0.704	0.086
BG2	Whole rock	-0.188	0.025
BG3	Whole rock	-0.109	0.018
BG4	Whole rock	-0.184	0.029
Duplicated		-0.180	0.030
BG5	Whole rock	-0.089	0.045
BG6	Whole rock	-0.035	0.031
Silicate lava			
HT1	Whole rock	-0.332	0.029
HT2	Whole rock	-0.417	0.052
HT3	Whole rock	-0.355	0.043
HT4	Whole rock	-0.064	0.025
HT5	Whole rock	-0.424	0.050
Duplicated		-0.448	0.068
HT6	Whole rock	0.090	0.048
Duplicated		0.085	0.094
HT7	Whole rock	-0.355	0.060
Duplicated		-0.349	0.091
HT8	Whole rock	-0.142	0.034
HT11	Whole rock	-0.042	0.066
HT13	Whole rock	-0.332	0.036
Duplicated		-0.272	0.036
HT14	Whole rock	-0.324	0.032
Duplicated		-0.330	0.079
HT1	Phlogopite	-0.628	0.039
HT4	Phlogopite	-0.566	0.030
HT5	Phlogopite	-0.534	0.065
Duplicated		-0.511	0.035
Carbonatite			
FS01	Whole rock	-0.858	0.064
FS02	Whole rock	-0.258	0.036

This is the peer-reviewed, final accepted version for American Mineralogist, published by the Mineralogical Society of America.
The published version is subject to change. Cite as Authors (Year) Title. American Mineralogist, in press.
DOI: https://doi.org/10.2138/am-2022-8898. http://www.minsocam.org/

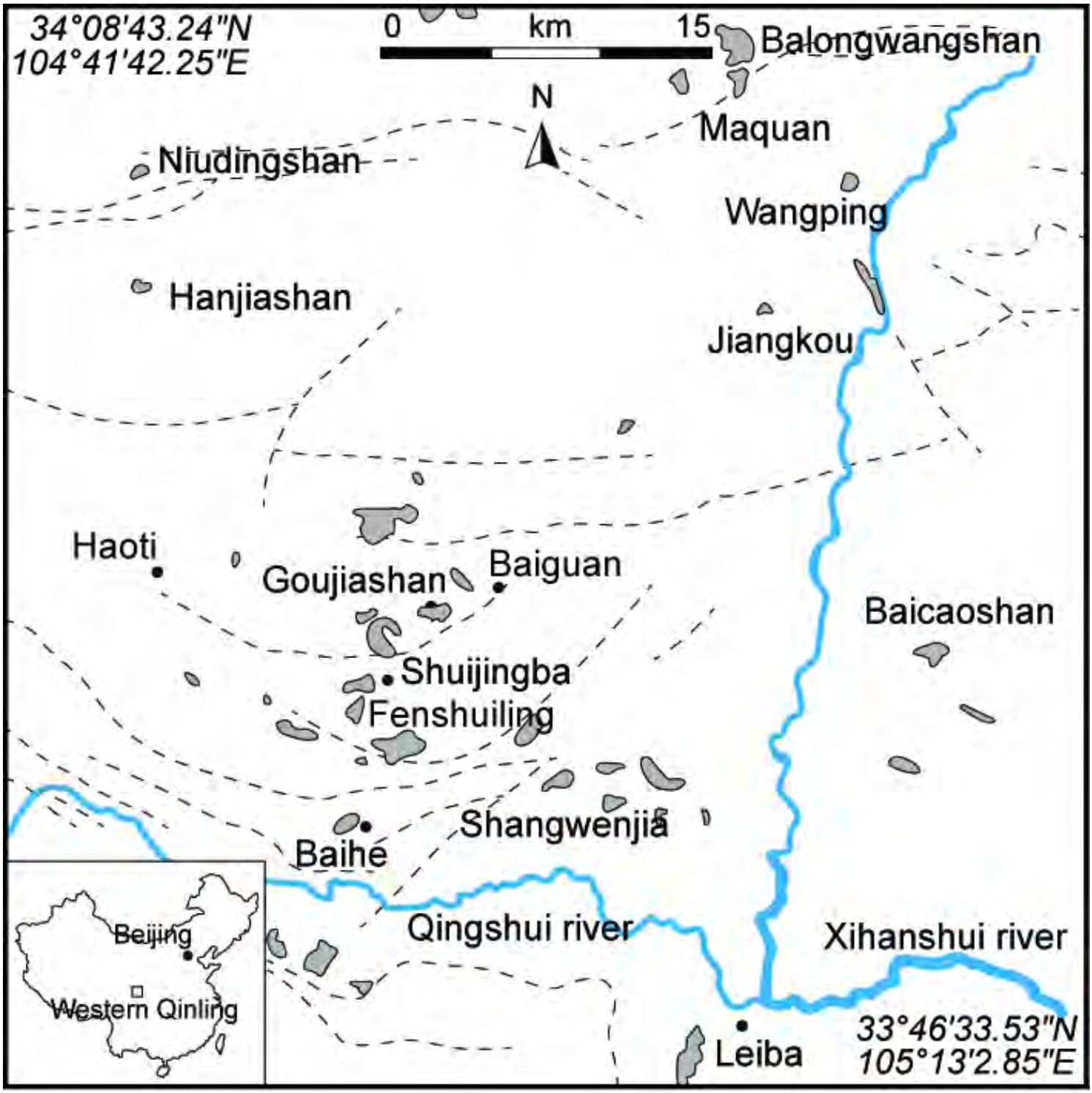

Fig. 1

This is the peer-reviewed, final accepted version for American Mineralogist, published by the Mineralogical Society of America.
The published version is subject to change. Cite as Authors (Year) Title. American Mineralogist, in press.
DOI: https://doi.org/10.2138/am-2022-8898. http://www.minsocam.org/

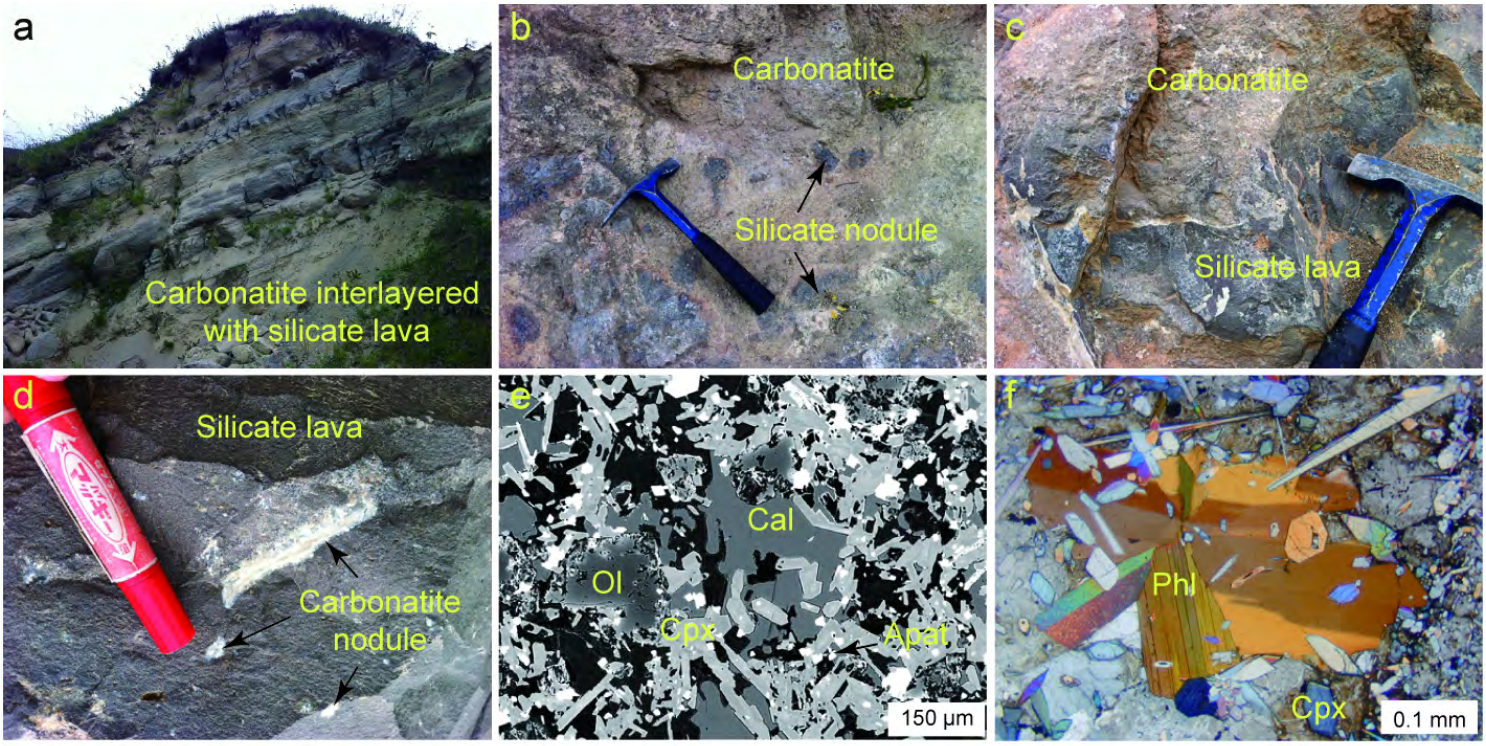

Fig. 2

This is the peer-reviewed, final accepted version for American Mineralogist, published by the Mineralogical Society of America.
The published version is subject to change. Cite as Authors (Year) Title. American Mineralogist, in press.
DOI: https://doi.org/10.2138/am-2022-8898. http://www.minsocam.org/

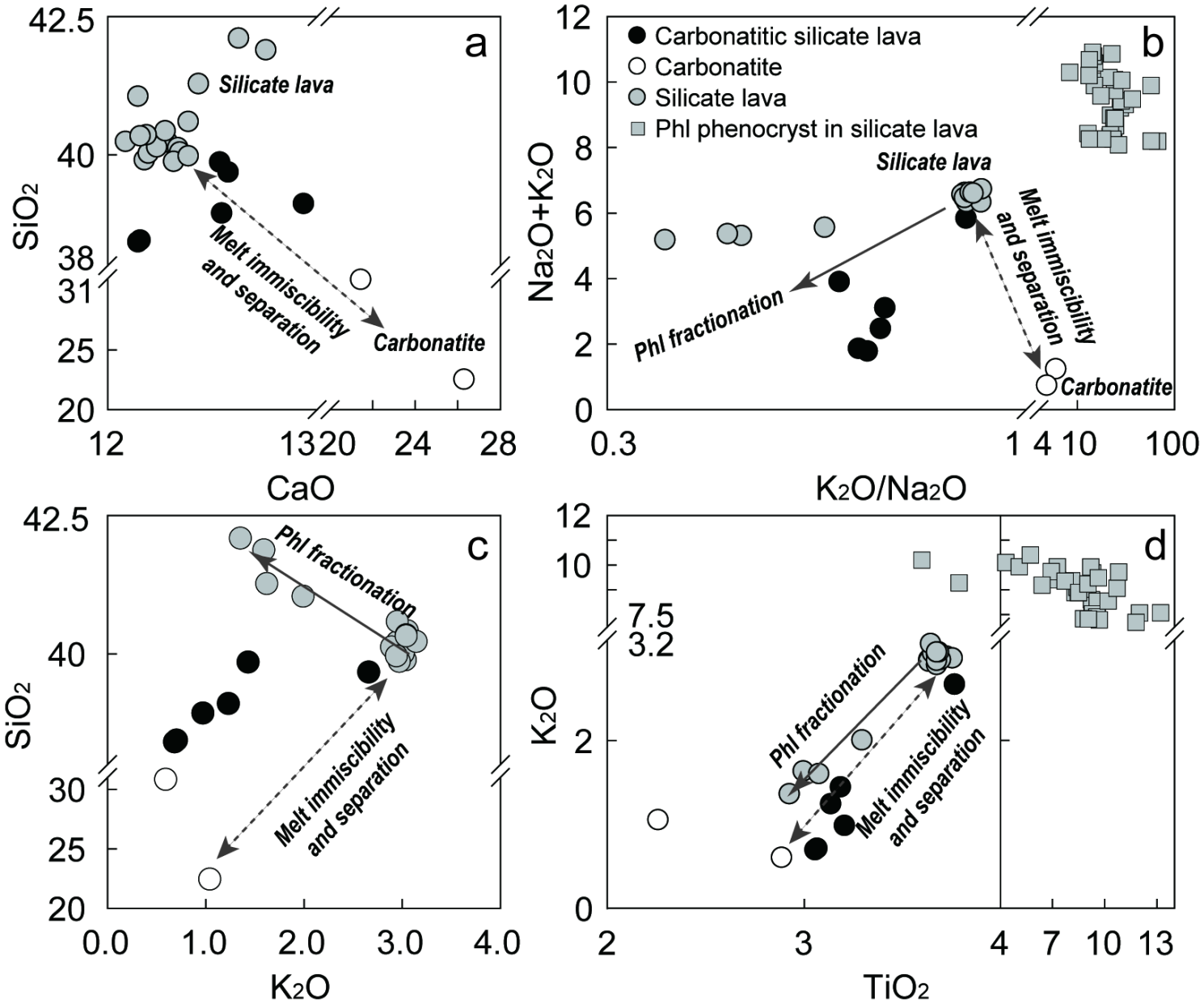

Fig. 3

This is the peer-reviewed, final accepted version for American Mineralogist, published by the Mineralogical Society of America.
The published version is subject to change. Cite as Authors (Year) Title. American Mineralogist, in press.
DOI: https://doi.org/10.2138/am-2022-8898. http://www.minsocam.org/

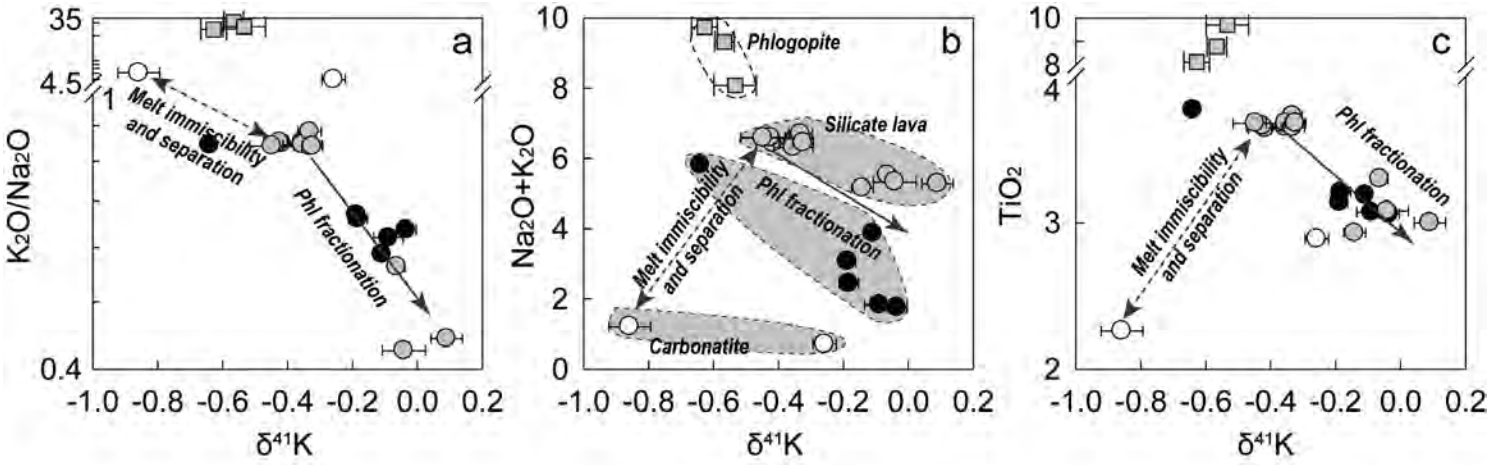

Fig. 4

This is the peer-reviewed, final accepted version for American Mineralogist, published by the Mineralogical Society of America.
The published version is subject to change. Cite as Authors (Year) Title. American Mineralogist, in press.
DOI: https://doi.org/10.2138/am-2022-8898. http://www.minsocam.org/

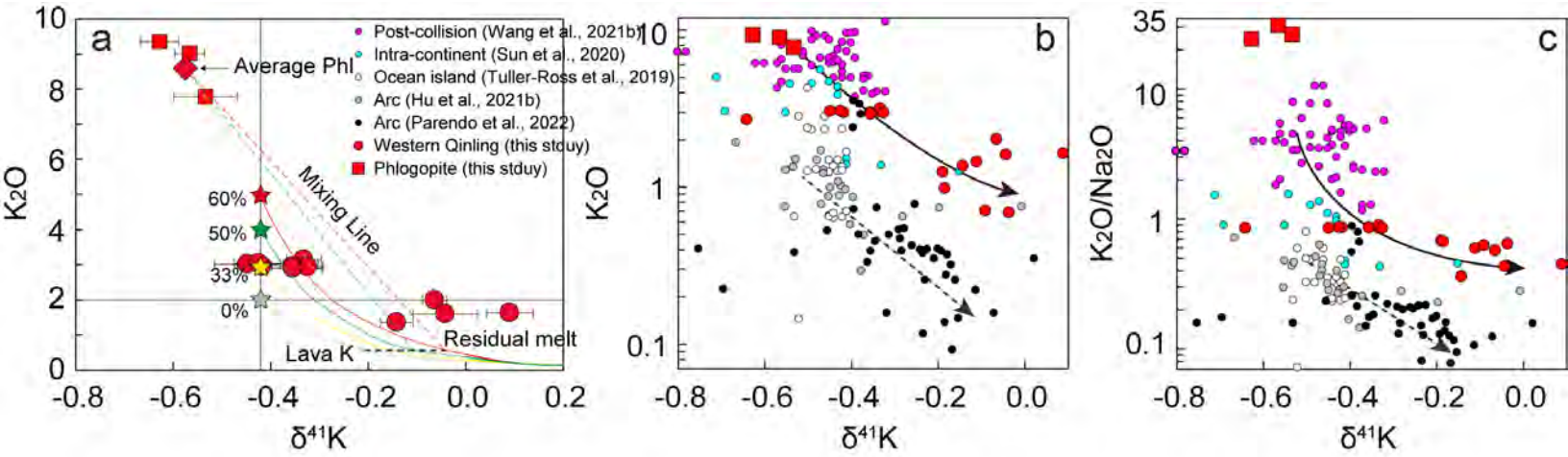

Fig. 5

This is the peer-reviewed, final accepted version for American Mineralogist, published by the Mineralogical Society of America.
The published version is subject to change. Cite as Authors (Year) Title. American Mineralogist, in press.
DOI: https://doi.org/10.2138/am-2022-8898. http://www.minsocam.org/

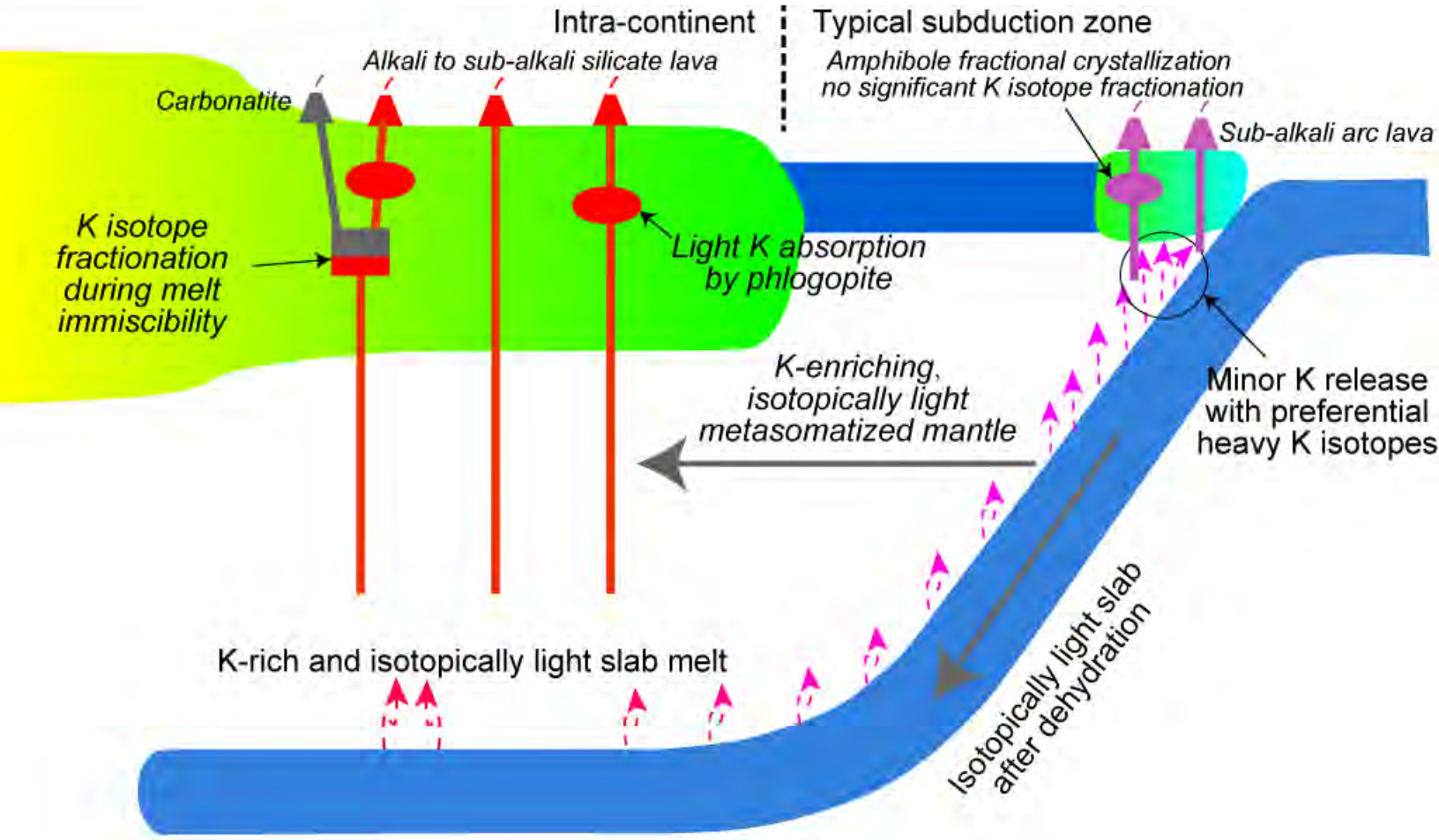

Fig. 6